**The American Journal of Human Genetics, Volume *103***

## Supplemental Data

# Mutations in Outer Dynein Arm Heavy Chain *DNAH9* Cause Motile Cilia Defects and Situs Inversus

**Mahmoud R. Fassad, Amelia Shoemark, Marie Legendre, Robert A. Hirst, France Koll, Pierrick le Borgne, Bruno Louis, Farheen Daudvohra, Mitali P. Patel, Lucie Thomas, Mellisa Dixon, Thomas Burgoyne, Joseph Hayes, Andrew G. Nicholson, Thomas Cullup, Lucy Jenkins, Siobhán B. Carr, Paul Aurora, Michel Lemullois, Anne Aubusson-Fleury, Jean-François Papon, Christopher O'Callaghan, Serge Amselem, Claire Hogg, Estelle Escudier, Anne-Marie Tassin, and Hannah M. Mitchison**

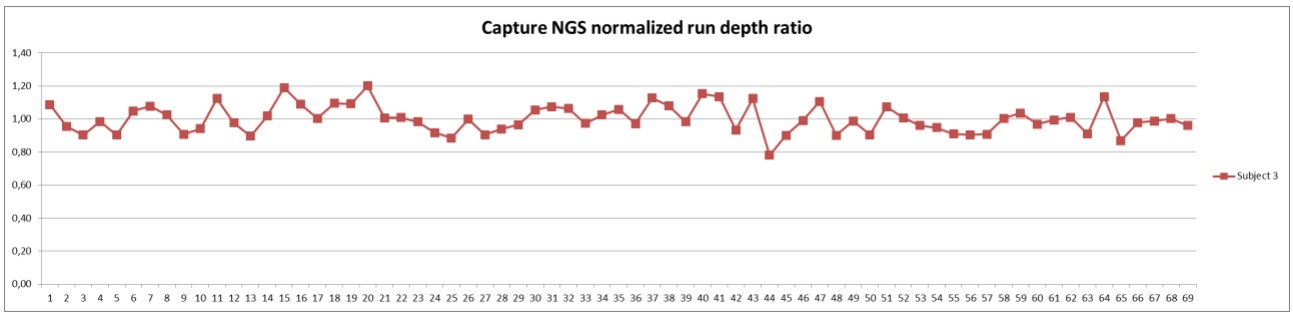


**B**

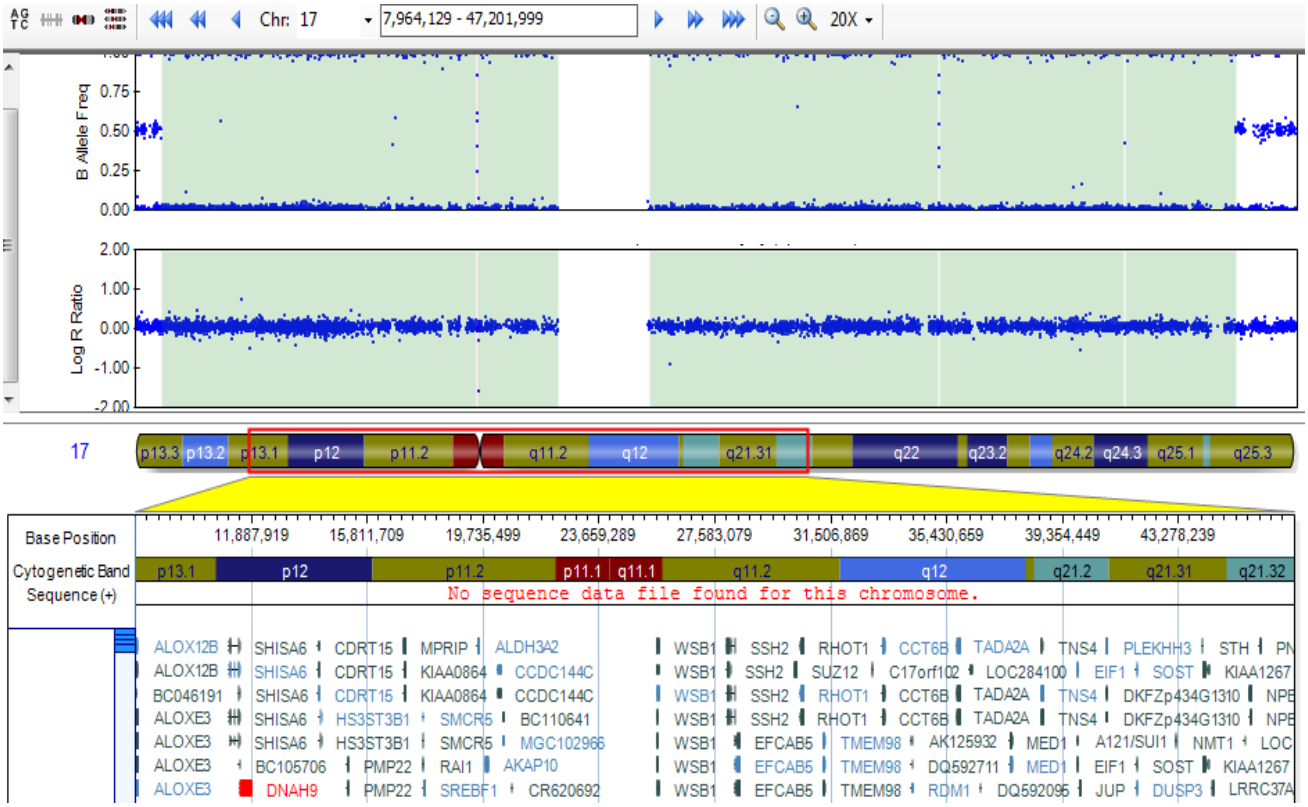


**Figure S1. The complex allele in affected individual 3.II.1 arises from two homozygous *DNAH9* mutations.** (A) Normalized *DNAH9* NGS depth ratio for subject 3.II.1. All 69 coding exons showed sequencing depth ratio ranging from 0.78 to 1.20 which confirms that subject 3.II.1 is homozygous for the predicted p.[(Lys1881Glu;Arg2965His)] complex allele (and is not hemizygous). Targeted NGS panel sequencing depths have been normalized between the probe-specific depth of 24 patients from the same run. (B) SNP array CNV analysis data for subject 3.II.1 (GenomeStudio viewer, Illumina). *DNAH9* is included in a large pericentromeric 36.4Mb homozygosity region on chromosome 17 which again highlights that subject 3.II.1 is homozygous for the p.[(Lys1881Glu;Arg2965His)] complex allele (and not hemizygous). The homozygous region is highlighted in green in the first (B allele frequency data) and second (Log R for CNV analysis) panel. Null or 1 value for B allele frequency indicates homozygosity or hemizygosity for allele B; null values for LogR indicate 2 copies for the assessed SNP.

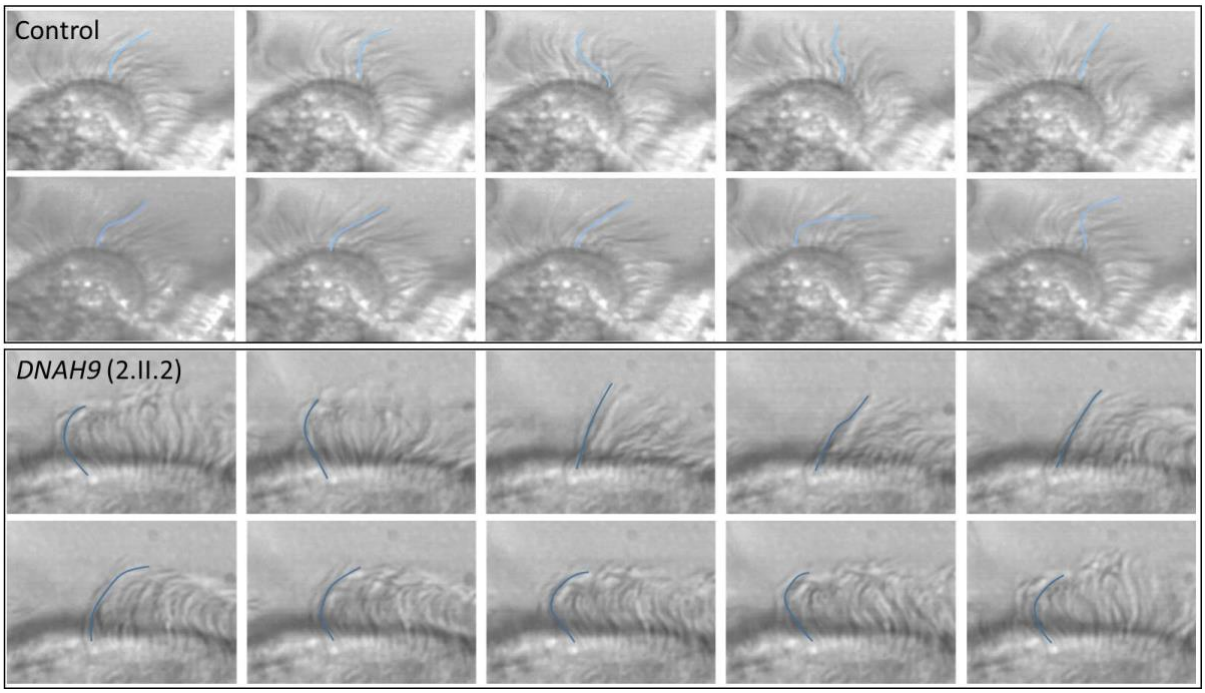


**Figure S2. Defective ciliary beat pattern in an individual with *DNAH9* mutations.** Consecutive images captured from HSVM across the course of a full ciliary beat, shown in panels 1-10 above for a healthy control and 11-20 below for affected individual 2.II.2 with *DNAH9* mutations.

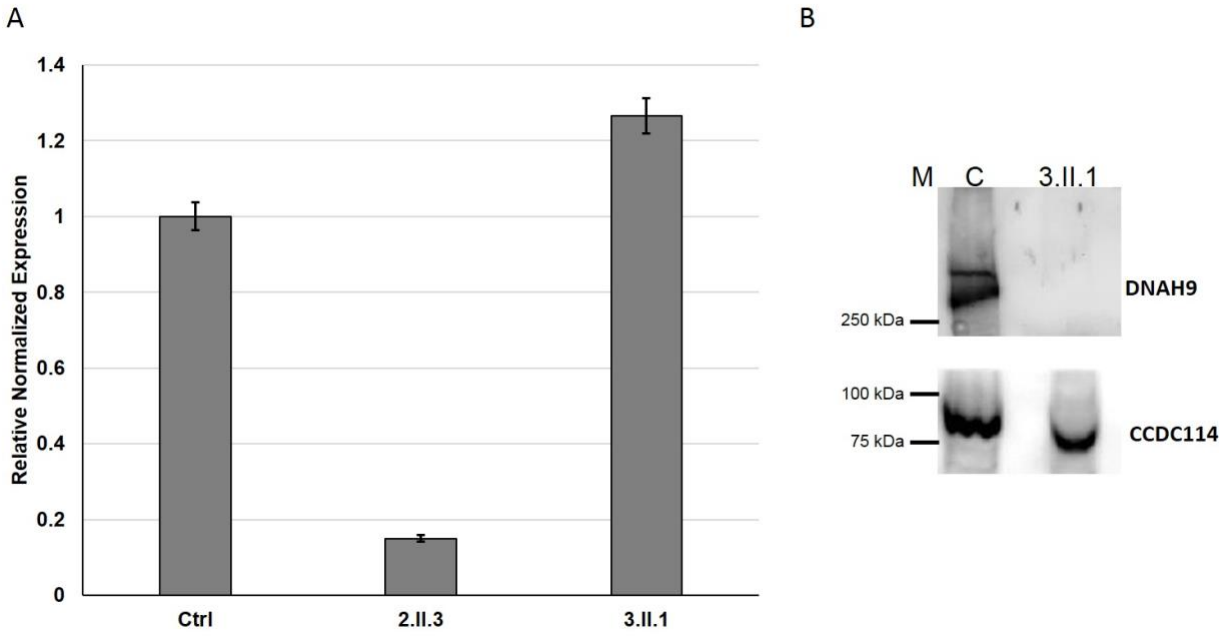


**Figure S3. DNAH9 transcript and protein levels in ciliated nasal samples from individuals with *DNAH9* mutations.** (A) Quantitative RT-PCR analysis of DNAH9 expression in whole nasal samples obtained from different individuals carrying *DNAH9* mutations. The RTqPCR analysis compared expression of *DNAH9* to that of *GAPDH* as a housekeeping gene for the normalisation. Error bars indicate SEM. (B) Western blotting of the nasal sample in affected individual 3.II.1 showed a complete lack of DNAH9 in the nasal sample compared to normal levels of another protein associated with PCD mutations, CCDC114, a component of the outer dynein arm docking complex. M, molecular marker. C, Ctrl, healthy individual.

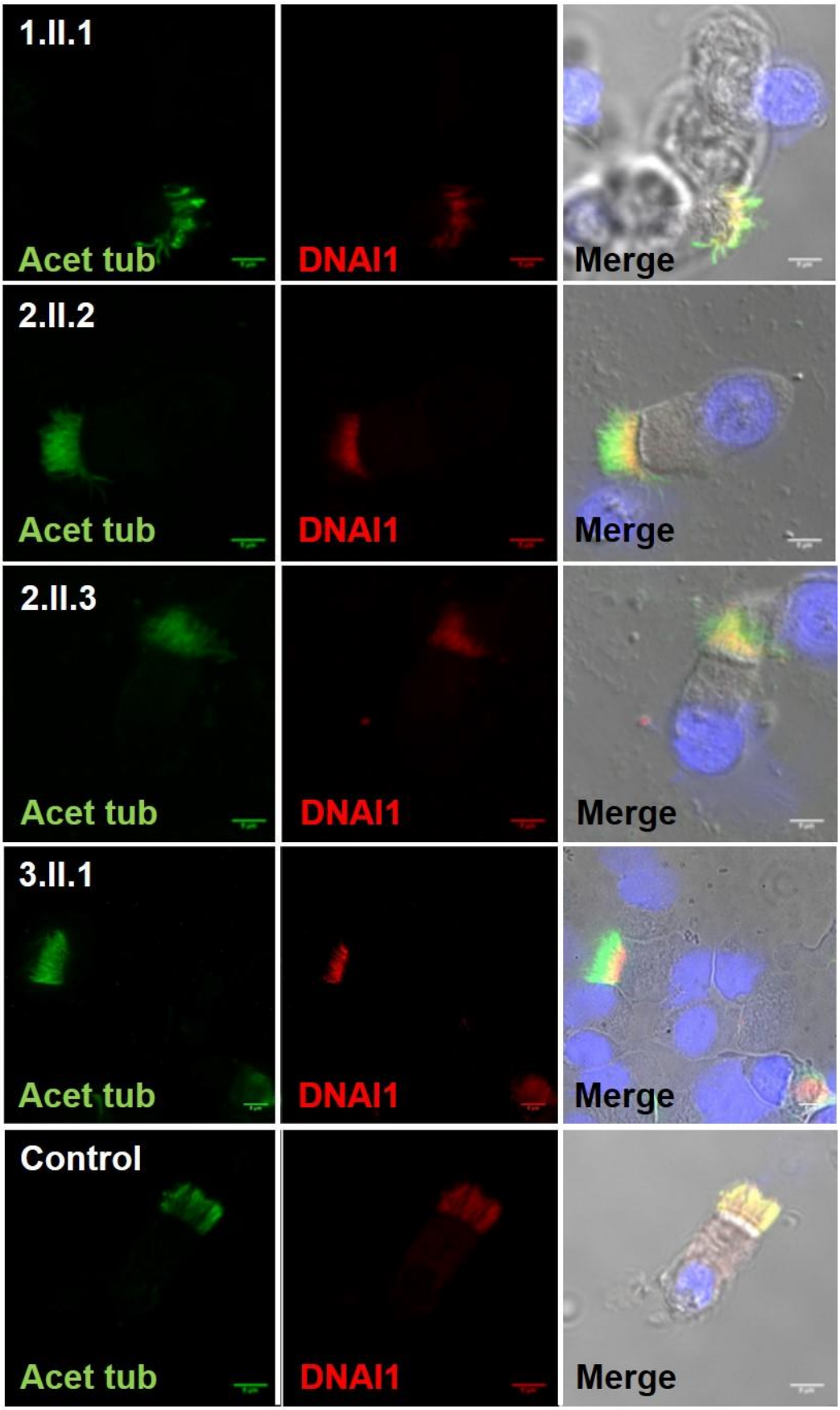


**Figure S4. Immunostaining of DNAI1 in cilia from individuals with *DNAH9* mutations.** Nasal epithelial cells were stained with a marker of the ciliary axoneme (acetylated tubulin, green), the ODA marker DNAI1 (red) and the nucleus (DAPI, blue). DNAI1 staining is reduced in a regional manner being lost only from the cilia distal regions. Scale bars, 5 μM.

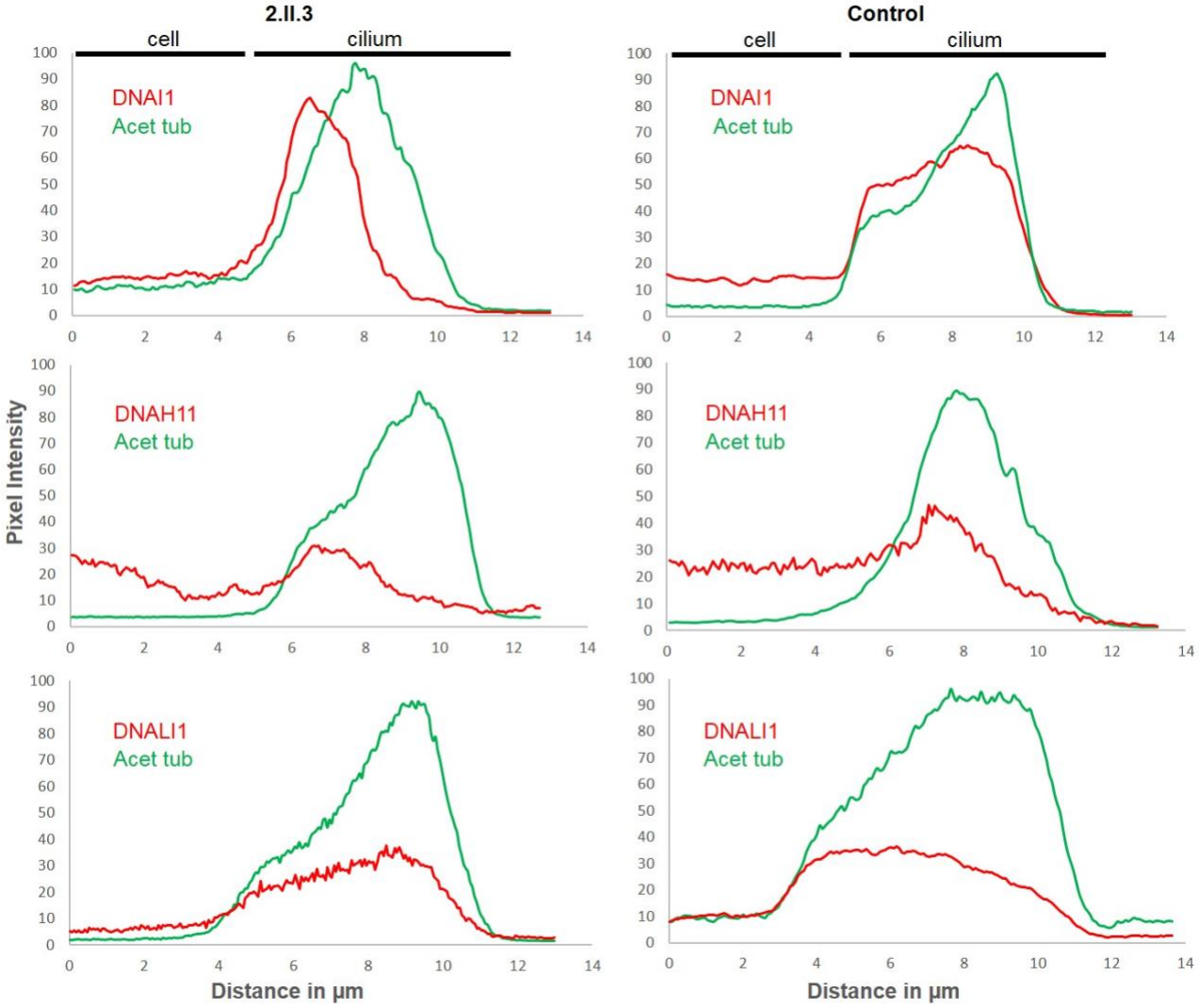


**Figure S5. Quantification of dynein arm components along the length of the cilium in an individual with *DNAH9* mutations.** Graphs show signal of ODA proteins DNAI1, DNAH11 compared to the inner dynein arm marker DNALI1. Signal was quantified by plotting the pixel intensity in images across profile plots of immunofluorescent images of antibody labelled cilia, in individual 2.II.3 (left) and a healthy individual (right). Like DNAH5 (Figure 2), DNAI1 is present mainly in the proximal part of the cilia and reduced in the distal part, while DNAH11 and DNALI1 are unchanged in their distribution along the axoneme.

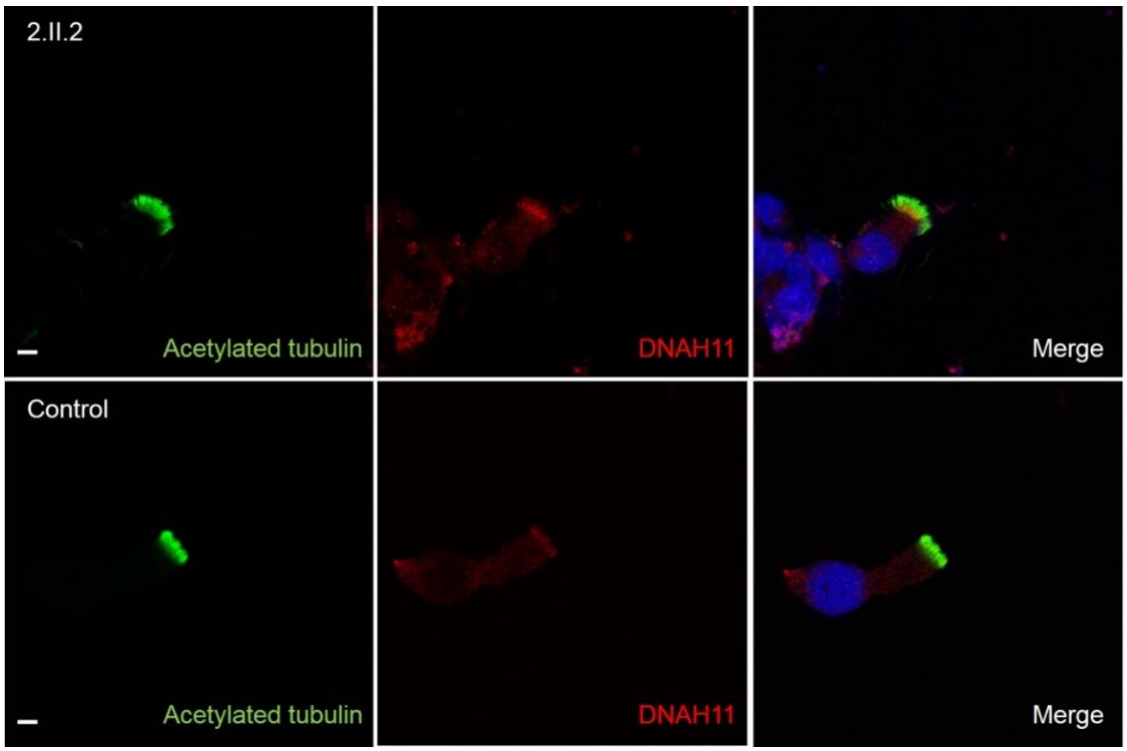


**Figure S6. Immunostaining of DNAH11 in an affected individual (2.II.2) with *DNAH9* mutations.** Nasal epithelial cells from 2.II.2 and a healthy control were stained with a marker of the ciliary axoneme (acetylated tubulin, green), the outer dynein arm beta heavy chain marker DNAH11 (red) and the nucleus (DAPI, blue). DNAH11 localises to the proximal cilia region similarly to controls. [7; 8] Scale bars, 5 μM.

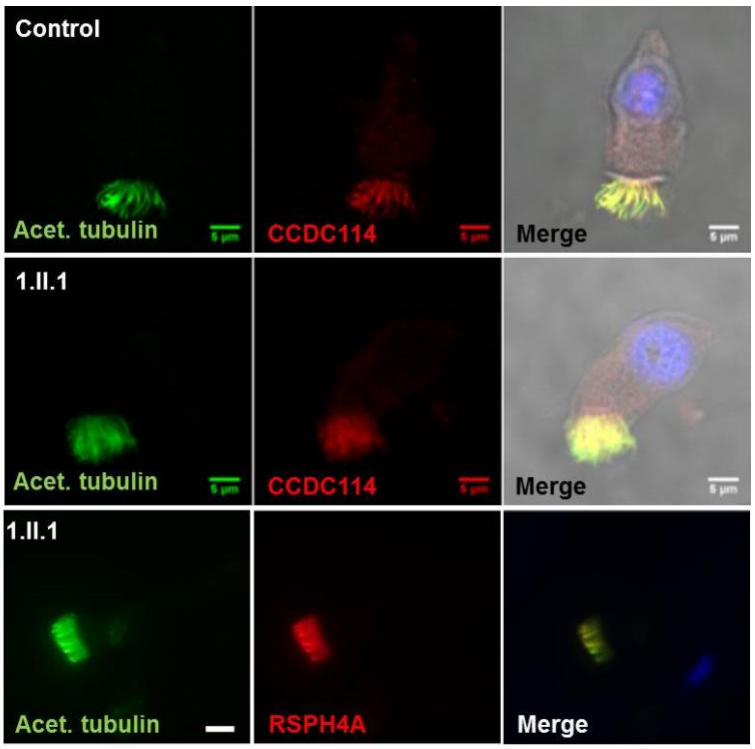


**Figure S7. Immunostaining of CCDC114 and RSPH4A in cilia from individuals with *DNAH9* mutations.** Nasal epithelial cells were stained with a marker of the ciliary axoneme (acetylated tubulin, green), the ODA docking complex marker CCDC114 or radial spoke marker RSPH4A (red) in addition to the nucleus (DAPI, blue). CCDC114 and RSPH4A distribution is undisturbed in cilia from individuals with *DNAH9* mutations. Scale bars, 5 μM.

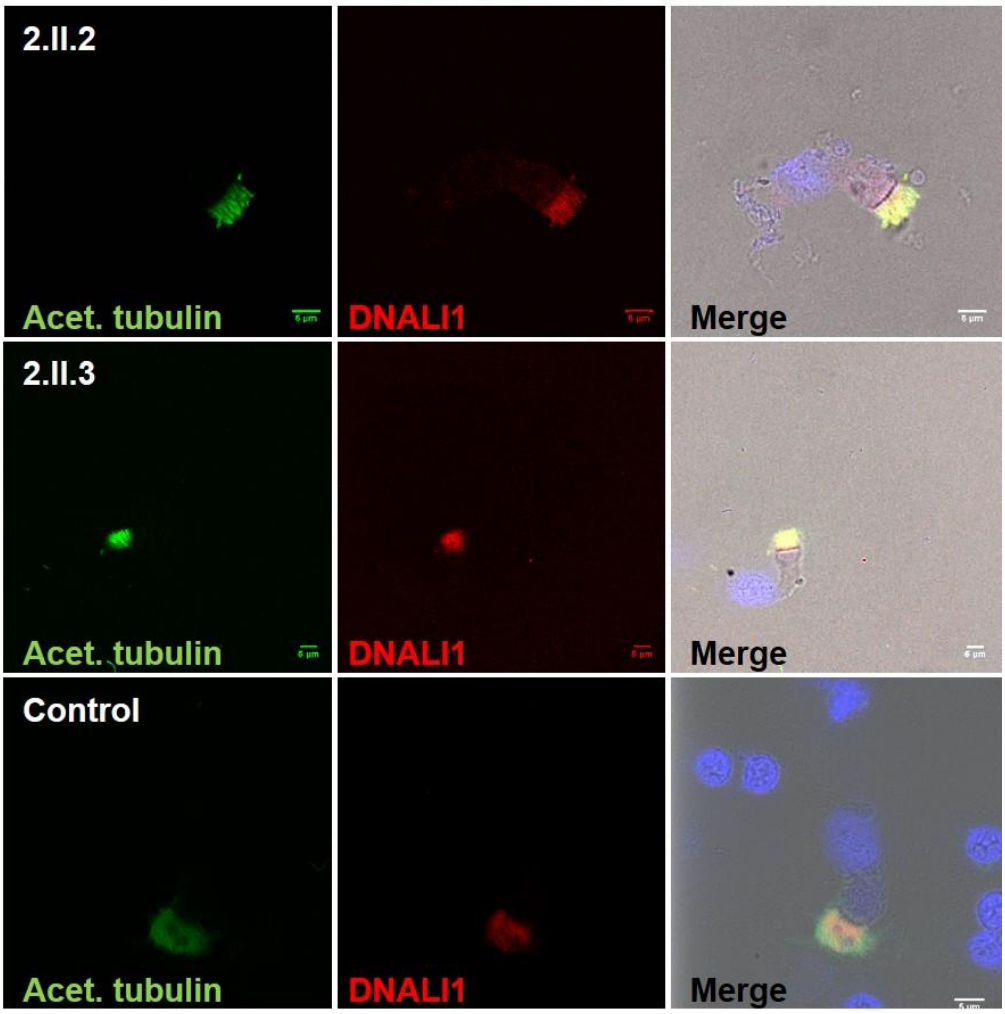


**Figure S8. Immunostaining of DNALI1 in cilia from individuals with *DNAH9* mutations.** Nasal epithelial cells were stained with a marker of the ciliary axoneme (acetylated tubulin, green), the IDA marker DNALI1 (red) and the nucleus (DAPI, blue). DNALI1 distribution is undisturbed in individuals with *DNAH9* mutations. Scale bars, 5 μM.

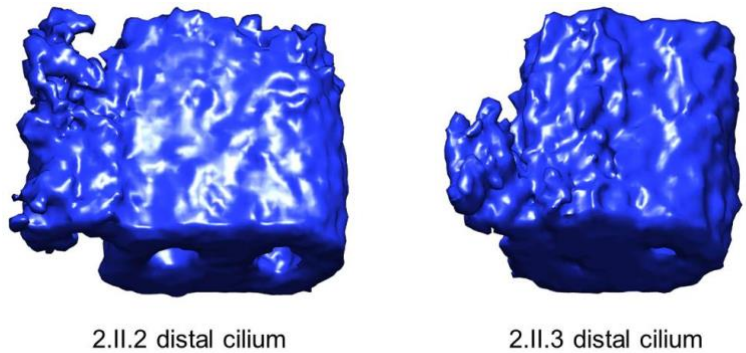


**Figure S9. Electron tomography and averaging of ODAs in the distal cilia region of individuals with *DNAH9* mutations** 3D models of the ODA falsely coloured blue for visualisation were generated as described in the main text, for the affected siblings 2.II.2 and 2.II.3. Using PEET analysis, transmission electron microscope tomograms taken from an area with >6 ciliary cross sections (54 microtubular doublets) were combined into a single model, showing reduced volume of ODA from the distal cilia.

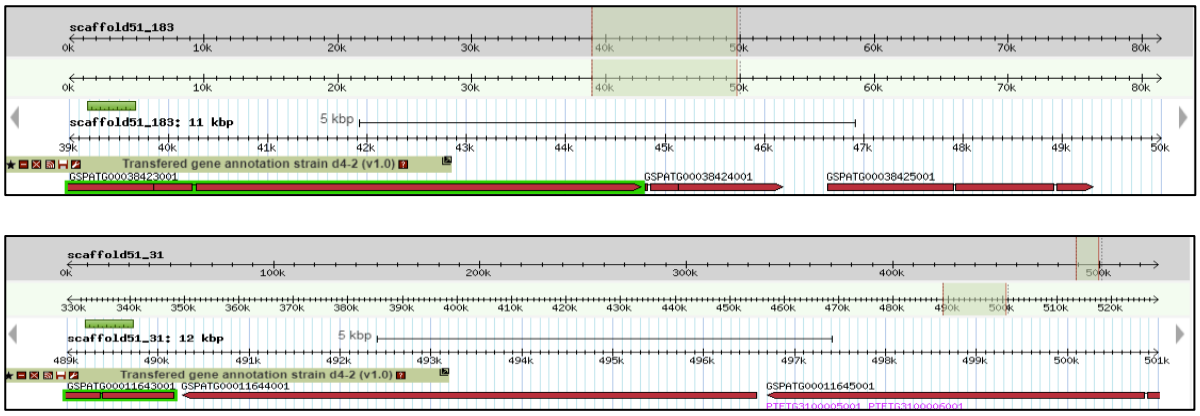


**Figure S10. Alignments of two human DNAH9 orthologs in *Paramecium***. Snapshots of GBrowse tool in *Paramecium* DB, showing regions of the *Paramecium* genome which have predicted open reading frames with homology to human DNAH9. Two DNAH9 orthologs are present in *Paramecium* on different genome scaffolds. This is presumed to result from genome duplication. These are contained within the gene sequences *GSPATG00038423001*, *GSPATG00038424001*, *GSPATG00038425001* (upper panel) and *GSPATG00011643001*, *GSPATG00011644001*, *GSPATG00011645001* (lower panel).

| | |
|---|---|
| **Volume (mL)** | 3.9 |
| **Concentration (million per mL)** | 2 |
| **Vitality (%)** | 50 |
| **Sperm morphology (% of abnormal spermatozoa)** | 100 |
| **Motility (%):** | |
| Type a (progressive, normal) | 5 |
| Type b (progressive, slow) | 10 |
| Type c (non-progressive motility) | 13 |
| Type d (immotile) | 72 |

**Table S1. Sperm analysis for individual 3.II.1.**

| Individual | Frequency (Hz) | Angle (°) | Distance/s (µm) | Surface/s (µm²) |
|---|---|---|---|---|
| 2.II.2 | 5.0 ±0.6 | 71 ±20.0 | 30.9 ±5.4 | 79.1 ±11.8 |
| 2.II.3 | 6.6 ±0.3 | 54 ±17.0 | 39.7 ±14.6 | 124.4 ±48.3 |
| 3.II.1 | 5.0 ±0.9 | 58 ±30.0 | 26.8 ±16.1 | 74.2 ±54.8 |
| Non-PCD controls (n=15) | 8.9 ± 2.0 | 71.6±6.6 | 66.7±14.2 | 208.6±49.2 |

**Table S2. Cilia beating parameters measured by HSVM in individuals with *DNAH9* mutations versus controls.** Data are expressed as mean ±SD.

| Primer ID | (5'- Sequence -3') |
|---|---|
| **Sanger Sequencing for c.12367G>A mutation** | |
| Fwd | GAAGCGTCCCTCTCTTGTGG |
| Rev | TTAAACAGGGCAGGCTTGGG |
| **Sanger Sequencing for c.8708-2A>G mutation** | |
| Fwd | AGACATGGTGTCTGTCCAGC |
| Rev | CCAGACCCTGGCTCTTGAC |
| **Sanger Sequencing for c.10193G>T mutation** | |
| Fwd | GCCGTGCAGAACTTCAAACA |
| Rev | GGATGAGTGTGCAGGAGGAC |
| **Sanger Sequencing for c.5641A>G mutation** | |
| Fwd | GAACCTGTCAGGGAGCCTCT |
| Rev | GCTGTGCTTCCTCATCACAT |
| **Sanger Sequencing for c.8894G>A mutation** | |
| Fwd | TGTGCTTCCCAATCTTCTGG |
| Rev | CTAACATCCTGGACAGGGAAT |
| **RT-PCR for characterization of splice acceptor variant** | |
| Fwd (Exon 41) | CACTGATCGATCTGGCCCTC |
| Rev (Exon 47) | GGCTGACAGACTCCAATGCT |
| **qRT-PCR for characterization of transcript abundance** | |
| DNAH9 Fwd (Exon 61) | GGTGGACCCACTGAAGGATG |
| DNAH9 Rev (Exon 62) | CTTGCCCCAAAGACACGTTG |
| GAPDH Fwd | TGCACCACCAACTGCTTAGC |
| GAPDH Rev | GGCATGGACTGTGGTCATGAG |
| **qRT-PCR for *DNAH9* orthologs knockdown in *Paramecium*** | |
| Ortholog1_Fwd | TCCAGCACCTAGATCAGGTC |
| Ortholog1_Rev | CTGGTTTCTTCTCGCTGTCT |
| Ortholog2_Fwd | TTCCAGCACCTAGGTCGGGCCA |
| Ortholog2_Rev | CTGGCTTTTTCTCACTATCC |
| GAPDH_Fwd | GAGAGCCGGAAGAGCTGCTA |
| GAPDH_Rev | TGGTGGAACTCTGAAGGCCATA |

**Table S3. Primers used in the study**

| Antigen | Antibody | Host species | Source | Application |
|---|---|---|---|---|
| DNAH9 | HPA052641 | Rabbit | Sigma-Aldrich | IF (1:500) |
| DNAH5 | HPA037470 | Rabbit | Sigma-Aldrich | IF (1:800) |
| DNAH11 | AB126571 | Rabbit | Abcam | IF (1:200) |
| DNALI1 | HPA028305 | Rabbit | Sigma-Aldrich | IF (1:200) |
| DNAI1 | HPA021649 | Rabbit | Sigma-Aldrich | IF (1:200) |
| RSPH4A | HPA031196 | Rabbit | Sigma-Aldrich | IF (1:400) |
| GAS8 | HPA041311 | Rabbit | Sigma-Aldrich | IF (1:500) |
| Acetylated tubulin | T7451 | Mouse | Sigma-Aldrich | IF (1:500) |
| Acetylated tubulin | YF488 | Mouse | Proteintech | IF (1:500) |
| CCDC114 | HPA042524 | Rabbit | Sigma-Aldrich | IF (1:500) |

**Table S4. Primary antibodies used in the study**

| Antibody | Host Species | Source | Application |
|---|---|---|---|
| Alexa 488, 594 – conjugated anti-rabbit IgG (H+L) | Goat | Invitrogen (Molecular Probes) | IF (1:1000) |
| Alexa 488, 594 – conjugated Anti-mouse IgG1 | Goat | Invitrogen (Molecular Probes) | IF (1:1000) |

**Table S5. Secondary antibodies used in the study**

**Supplementary Materials and Methods**

**Subjects and families**

Signed and informed consent was obtained from all participants before history recording, blood drawing and nasal biopsy, using protocols approved by the ethics review boards of the Institute of Child Health/Great Ormond Street Hospital, London (UK) (08/H0713/82) and the Comité de Protection des Personnes CPP Ile-de-France III (France) (CPP07729 and CPP02748). Affected individuals were diagnosed with PCD through standard diagnostic screening, according to European Respiratory Society diagnostic guidelines. [1]

**Genetic analysis**

Targeted next generation sequencing panels used Agilent SureSelectQXT technology for UK screened cases 1.II.1, 2.II.1, 2.II.2 or Roche SeqCap EZ Choice for case 3.II.1. Primers used for Sanger sequencing are listed in Table S3.

**Immunofluorescence quantification of dynein staining in cilia**

Antisera used in immunofluorescence are listed in Table S4 and S5 with methods as previously described. [2] For quantification of dynein distribution along cilia, the DNAH5, DNAI1, DNAH11, DNALI1 signal versus acetylated tubulin signal were quantified in ImageJ (Java based open source software developed by the NIH) using the profile plot function. A linear region of interest was drawn through the centre of each stained ciliated epithelial cell on a calibrated image. The pixel intensity for each channel was plotted against the position on the region of interest in µM, based upon 10 profile plots.

**Western blot of nasal epithelial cells**

Airway epithelial cells obtained by airway brushing from affected individual 3.II.1 and control individual were suspended in ice-cold RIPA lysis buffer, sonicated and cleared by 10 minutes of centrifugation at 1000g, 4°C.Cell lysates were loaded on SDS-PAGE 4-12% gradient gel (Invitrogen XV04120PK20) to be analyzed by western blotting with anti-DNAH9 or anti-CCDC114 antibodies (Table S4, 1/200) incubated overnight at 4°C. The secondary antibody (SIGMA A0545, 1/5000) was incubated for 45 min at RT. Proteins were detected using Amersham ECL Select Western Blotting Detection Reagent (GE healthcare) according to the manufacturer's recommendations.

**Ciliary beating quantification**

Ciliary beating analysis was performed by high-speed videomicroscopy (according to the protocols described by Chilvers et al and Papon et al). [3; 4] In brief, beating ciliated edges were recorded with a high-speed digital camera (with a 100× objective at a rate between 355-500 frames per second. Cilia able to be followed during a complete beating cycle were then selected in distinct areas. We collected several measurements made on cilia in order to determine the following objective parameters: the ciliary beat frequency, the beating angle, the distance and the surface travelled by the tip of the cilium per second.

Microbead motion was studied according to the method developed by Bottier et al. [5] to assess the flow generated by ciliary beating, by tracking the displacement of microbeads used as markers of the flow. This method, backed by a theoretical model of the flow motion induced by cilia beating allows to infer the shear stress exerted by the cilia on the medium. This shear stress is shown to be an index for characterizing the efficiency of ciliary beating in mucociliary clearance.[6]

***Paramecium* knockdown**

The *DNAH9 Paramecium* coding sequence used is 737bp long. It is 100% identical to sequences on two different parts of the genome, scaffold 31 and scaffold 183, as shown in Figure S10. Both the *Paramecium* genes have ORFs that show homology to human DNAH9, as a result of genome duplication in *Paramecium*. RNAi was performed as previously described, [2] using the sequence:

5'CGTTAGTACTAGAGATTTGTATGGTTACAATTTACCAACAAAGGAATGGAAAGATGGTTTAGT
TTCAAAGGTTTTGAGATCTCTAAGTGAAATTCAAGATGTTAATCCTAAATGGATATTACTTGAT
GGAGATTTAGATGCTAATTGGATTGAGTCTATGAATTCAGTGATGGATGACAATAAGATATTGA
CATTGGCAAATAATGAAAGAATTCCATTGAAACCACACATGAGAATGCTTTTTGAAATCAGAG
ATCTTCGTTTTGCTACTCCTGCCACAGTGTCTAGAGCTGGTATCTTATATATTTCAGATGACAAG
GGGTATTAATGGAGAGCCTACGTGAAATCATGGGTTAAGAATAACTTTAATGATGATAAATTTA
AATAAGATTTACAAAAACTATTTGATAGATATATTGAAGGTACTTTACTATTCTTAAAGAAACA

TTGTAAGACTTTGATTCCAGTCAATCCAATTTCTATGATTATCTCATTATGCAAAGCCTTATTGC
CATTATTATAAGGAGAAGTGAAGAATATGGAATATCATTTCGTGTATTGCTGTGTTTGGGCTAT
TGGAGGTGTTTTATCTGAAAAAGACTCCATTGATTATCGTAAAGATTTCTCTAATTGGTGGAAA
GGTGAATGGAAGACTTCAGTAAAATTCCCAAGTAAGGGTACAGTATTTGATTACTTTGTTGAAT
AAAATTCAGAGAATGTTAAATTCGATGAATGGG-3'.

**Supplementary references**


1. Lucas, J.S., Barbato, A., Collins, S.A., Goutaki, M., Behan, L., Caudri, D., Dell, S., Eber, E., Escudier, E., Hirst, R.A., et al. (2017). European Respiratory Society guidelines for the diagnosis of primary ciliary dyskinesia. Eur Respir J 49.
2. Fassad, M.R., Shoemark, A., le Borgne, P., Koll, F., Patel, M., Dixon, M., Hayward, J., Richardson, C., Frost, E., Jenkins, L., et al. (2018). C11orf70 Mutations Disrupting the Intraflagellar Transport-Dependent Assembly of Multiple Axonemal Dyneins Cause Primary Ciliary Dyskinesia. Am J Hum Genet 102, 956-972.
3. Papon, J.F., Bassinet, L., Cariou-Patron, G., Zerah-Lancner, F., Vojtek, A.M., Blanchon, S., Crestani, B., Amselem, S., Coste, A., Housset, B., et al. (2012). Quantitative analysis of ciliary beating in primary ciliary dyskinesia: a pilot study. Orphanet J Rare Dis 7, 78.
4. Chilvers, M.A., Rutman, A., and O'Callaghan, C. (2003). Functional analysis of cilia and ciliated epithelial ultrastructure in healthy children and young adults. Thorax 58, 333-338.
5. Bottier, M., Blanchon, S., Pelle, G., Bequignon, E., Isabey, D., Coste, A., Escudier, E., Grotberg, J.B., Papon, J.F., Filoche, M., et al. (2017). A new index for characterizing micro-bead motion in a flow induced by ciliary beating: Part I, experimental analysis. PLoS Comput Biol 13, e1005605.
6. Bottier, M., Pena Fernandez, M., Pelle, G., Isabey, D., Louis, B., Grotberg, J.B., and Filoche, M. (2017). A new index for characterizing micro-bead motion in a flow induced by ciliary beating: Part II, modeling. PLoS Comput Biol 13, e1005552.
7. Dougherty, G.W., Loges, N.T., Klinkenbusch, J.A., Olbrich, H., Pennekamp, P., Menchen, T., Raidt, J., Wallmeier, J., Werner, C., Westermann, C., et al. (2016). DNAH11 Localization in the Proximal Region of Respiratory Cilia Defines Distinct Outer Dynein Arm Complexes. American Journal of Respiratory Cell and Molecular Biology 55, 213-224.
8. Shoemark, A., Burgoyne, T., Kwan, R., Dixon, M., Patel, M.P., Rogers, A.V., Onoufriadis, A., Scully, J., Daudvohra, F., Cullup, T., et al. (2018). Primary ciliary dyskinesia with normal ultrastructure: three-dimensional tomography detects absence of DNAH11. Eur Respir J 51.